J Biol Inorg Chem (2015) 20:531–540
DOI 10.1007/s00775-015-1238-6

ORIGINAL PAPER

Immobilized cytochrome *c* bound to cardiolipin exhibits peculiar oxidation state-dependent axial heme ligation and catalytically reduces dioxygen

Antonio Ranieri · Diego Millo · Giulia Di Rocco · Gianantonio Battistuzzi · Carlo A. Bortolotti · Marco Borsari · Marco Sola

Received: 22 September 2014 / Accepted: 27 December 2014 / Published online: 28 January 2015

Abstract Mitochondrial cytochrome *c* (cytc) plays an important role in programmed cell death upon binding to cardiolipin (CL), a negatively charged phospholipid of the inner mitochondrial membrane (IMM). Although this binding has been thoroughly investigated in solution, little is known on the nature and reactivity of the adduct (cytc–CL) immobilized at IMM. In this work, we have studied electrochemically cytc–CL immobilized on a hydrophobic self-assembled monolayer (SAM) of decane-1-thiol. This construct would reproduce the motional restriction and the nonpolar environment experienced by cytc–CL at IMM. Surface-enhanced resonance Raman (SERR) studies allowed the axial heme iron ligands to be identified, which were found to be oxidation state dependent and differ from those of cytc–CL in solution. In particular, immobilized cytc–CL experiences an equilibrium between a low-spin (LS) 6c His/His and a high-spin (HS) 5c His/− coordination states. The former prevails in the oxidized and the latter in the reduced form. Axial coordination of the ferric heme thus differs from the (LS) 6c His/Lys and (LS) 6c His/OH^- states observed in solution. Moreover, a relevant finding is that the immobilized ferrous cytc–CL is able to catalytically reduce dioxygen, likely to superoxide ion. These findings indicate that restriction of motional freedom due to interaction with the membrane is an additional factor playing in the mechanism of cytc unfolding and cytc-mediated peroxidation functional to the apoptosis cascade.

Keywords Cytochrome *c* · Cardiolipin · Electrochemistry · SERRS · Apoptosis · Dioxygen interaction

Abbreviations

cytc	Cytochrome *c*
ycc	Recombinant untrimethylated *Saccharomyces cerevisiae* yeast iso-1-cytochrome *c*
KtoA	Recombinant untrimethylated *Saccharomyces cerevisiae* yeast iso-1-cytochrome *c* variant K72A/K73A/K79A
CL	Cardiolipin

Introduction

The physiological function of mitochondrial cytochrome *c* (cytc) is strictly connected to its redox properties. These are in turn modulated by axial ligation and protein environment of the heme iron which are sensitive to solution properties and binding events [1–4]. This makes cytc a multi-task protein whose role can be modulated depending on the cell

Electronic supplementary material The online version of this article (doi:10.1007/s00775-015-1238-6) contains supplementary material, which is available to authorized users.

A. Ranieri · G. Di Rocco · C. A. Bortolotti · M. Sola (✉)
Department of Life Sciences, University of Modena and Reggio Emilia, Via Campi 183, 41125 Modena, Italy
e-mail: sola.marco@unimore.it; marco.sola@unimore.it

D. Millo
Department of Physics and Astronomy, LaserLaB Amsterdam, Vrije Universiteit, De Boelelaan 1083, 1081 HV Amsterdam, The Netherlands

G. Battistuzzi · M. Borsari (✉)
Department of Chemical and Geological Sciences, University of Modena and Reggio Emilia, via Campi 183, 41125 Modena, Italy
e-mail: marco.borsari@unimore.it

C. A. Bortolotti · M. Sola
CNR-NANO Institute of Nanoscience, Via Campi 213/A, 41125 Modena, Italy

status. The paradigm of this tunable functionality is constituted by the involvement of cytc in programmed cell death consequent to binding to cardiolipin (CL), a negatively charged phospholipid of the inner mitochondrial membrane (IMM), induced by early proapoptotic signals/events. Binding of cytc to CL blocks the electron transfer chain of mitochondrial respiration and imparts cytc with a significant peroxidase activity. This is followed by cytc ejection out of the mitochondrion where it promotes the apoptosis cascade [5, 6].

The changes in protein conformation and axial heme iron coordination upon cytc–CL adduct formation have been largely investigated. High- (HS) and low-spin (LS) six-coordinated (6c) conformers containing a His/His, His/Lys or His/OH^- axial binding set have been proposed for the oxidized state, while a five-coordinated (5c) HS His/− heme center has been suggested for the reduced state [7]. The latter form should also in principle be able to catalytically reduce dioxygen to the superoxide radical, but no evidence for this effect has been gained so far. All these studies were carried out in solution. However, specific recognition and binding of cytc to CL involve protein immobilization on IMM and the consequent restriction of its motional freedom. As this condition is likely not to be innocent in terms of protein conformational changes [8], here we studied through cyclic voltammetry the heme coordination features of the cytc–CL adduct (cytc–CL hereafter) immobilized on an electrode coated with a hydrophobic self-assembled monolayer (SAM) of decane-1-thiol (DT). This construct reproduces the motional restriction experienced by cytc upon binding to IMM. Insight into the nature of the axial ligands has been obtained from surface-enhanced resonance Raman (SERR) studies of immobilized cytc–CL under the same conditions. Immobilization of cytc–CL on the DT SAM can be ascribed to the dispersion interactions involving the three long alkyl chains of CL that do not penetrate the heme crevice of cytc [9], and to a possible conformational change of cytc upon CL binding that increases the hydrophobicity of the adduct [10, 11]. To our knowledge, this is the first voltammetric and spectroscopic investigation of ferric and ferrous cytc–CL in the immobilized state which leads to identification of the changes in axial heme ligands due to cytc adsorption and binding to CL. Previously, the reduction potential ($E^{\circ\prime}$) of cytc covalently bound to an anionic SAM interacting with CL-containing liposomes was found to shift negatively by up to 400 mV with respect to the $E^{\circ\prime}$ of the native conformer [12]. Moreover, a study of the electrochemical behavior of cytc immobilized on a CL-coated glassy carbon electrode revealed the existence of a minor form of immobilized cytc attributed to the adduct with CL [13].

Here, three cytc species were studied: the native protein from beef heart (bcc), the recombinant *Saccharomyces cerevisiae* yeast iso-1 protein (ycc) and its triple K72A/K73A/K79A variant (KtoA). These species were selected because cytc from beef heart plays indeed an apoptotic role while yeast cytc does not although it features a conserved heme environment including the axial His/Met ligation set [14]. The KtoA variant lacks all the lysine residues which are involved as 6th ligand of the heme iron under various conditions in vitro. Therefore, these species would in principle help drawing conclusions on the nature of the heme iron coordination in cytc–CL. Here, we found that the oxidation state-dependent axial ligand set and spin state of the heme iron and the reduction potential for immobilized cytc–CL are not the same as in solution. In particular, the coordination features of the ferric heme are affected most by immobilization. Moreover, we provide evidence for the as yet supposed ability of ferrous cytc–CL to catalytically reduce dioxygen.

Materials and methods

Materials

Wild-type (wt) recombinant untrimethylated *Saccharomyces cerevisiae* yeast iso-1-cytochrome *c* (ycc) and its variant K72A/K73A/K79A (KtoA) were expressed in *E. coli* and purified following the procedures described elsewhere [15–17]. In both cases, Cys102 was replaced by a threonine to avoid dimerization and minimize autoreduction without affecting the spectral and the functional properties of the protein [18, 19]. Beef heart cytochrome *c* (bcc) was purchased from Sigma-Aldrich and purified as ycc. All chemicals were of reagent grade. Decane-1-thiol (DT) and bovine cardiolipin (CL) were purchased from Sigma-Aldrich. Deionized water (MILLIQ) was used throughout.

Electrochemical measurements

A potentiostat/galvanostat mod. 273A (EG&G PAR, Oak Ridge, USA) was used to perform cyclic voltammetry (CV). Experiments were carried out at different scan rates (0.02–40 V s^{-1}) using a cell for small volume samples (0.5 mL) under argon. A 1 mm-diameter polycrystalline gold wire, a Pt sheet, and a saturated calomel electrode (SCE) were used as working, counter, and reference electrode, respectively. The electrical contact between the SCE and the working solution was achieved with a Vycor® (from PAR) set. All the reduction potentials reported here are referred to the standard hydrogen electrode (SHE), unless otherwise specified. The working gold electrode was cleaned by flaming under oxidizing conditions; afterwards, it was heated in concentrated KOH for 30 min, rinsed with water and subsequently cleaned by concentrated sulfuric

acid for 30 min. To minimize residual adsorbed impurities, the electrode was subjected to 20 voltammetric cycles between +1.5 and −0.25 V (vs. SCE) at 0.1 V s^{-1} in 1 M H_2SO_4. Finally, the electrode was rinsed in water and anhydrous ethanol. The Vycor® set was treated in an ultrasonic pool for about 5 min. SAM coating on the gold electrode was obtained by dipping the polished electrode into a 1 mM ethanol solution of DT for 12 h and then rinsing it with water. Cytochrome *c* solutions were freshly prepared before use in 10 mM Hepes buffer at pH 7 and their concentration (typically 10 μM) was carefully checked spectrophotometrically (Jasco mod. V-570 spectrophotometer). Protein adsorption on the DT SAM-coated Au electrode was achieved by dipping the functionalized electrode into a 1 μM protein solution at 4 °C for 1 h. cytc–CL adducts were obtained by mixing cytochrome *c* and CL to obtain a 10 μM protein and 300 μM CL solution (cytc/CL molar ratio 1:30) in 10 mM Hepes at pH 7, which was allowed to stand for 30 min. In these conditions, cytc is fully bound to CL [7, 19], as confirmed by the fluorescence spectra (Figure S1). Adduct adsorption on the DT-coated electrode was achieved by dipping the functionalized electrode into the above solution for 1 h at 4 °C. The CV measurements were made up in 10 mM Hepes buffer at pH 7. The electrochemical measurements were carried out avoiding the use of phosphate buffer. Indeed, phosphate ions at pH 7 are known to bind specifically to cytochrome *c* at the clustered surface lysines [20, 21], thereby altering the interaction with CL and the properties of the resulting adduct. The formal reduction potential $E^{\circ\prime}$ was taken as the midpoint between the anodic and cathodic peak potentials. CV measurements were performed at different scan rates *v* (from 0.02 to 40 V s^{-1}) and all the experiments were repeated at least five times. The reduction potentials were found to be reproducible within ±2 mV.

Resonance Raman (RR) and surface-enhanced resonance Raman spectroscopy (SERRS)

SERRS measurements on the electrode-immobilized cytochromes and their CL adducts were performed using a linearly moving spectroelectrochemical cell equipped with a flow system described elsewhere [22]. This configuration allows filling the cell with N_2-saturated buffer to minimize the presence of O_2 in contact with the working electrode. The working electrode was a 2.5-mm-diameter homemade nanostructured Ag electrode equipped with a removable Ag tip (SMARTIP Electrode, Mechanical Workshop of the VU University Amsterdam). The counter and the reference electrode were a Pt plate embedded inside the polymeric body of the spectroelectrochemical cell and a SCE (AMEL Instruments, Milan), respectively. Ag electrodes were polished and roughened as described previously [23]. SAM formation was achieved exposing the roughened electrode to a 1-mM ethanol solution of DT for 12 h. The procedure for immobilization of cytcs and their CL adducts on the Ag working coated with a DT SAM was identical to that used for the CV measurements. The reference electrode and the cell were kept at constant room temperature (19 °C) during all the experiments. The three-electrode system was controlled with a μAutolab potentiostat (Eco Chemie, Utrecht) supplied with the GPES 4.9 software for amperometric and voltammetric measurements. SERRS measurements were done by placing the spectroelectrochemical cell under a home-built Raman microscope operating in the backscattering configuration: a Zeiss microscope (D-7082 with a X16 objective, numerical aperture 0.60, working distance 2 mm) was coupled to an Andor Shamrock SR-303i-A single monochromator (Andor Technologies DV-420OE) with a mounted 2,400 g mm^{-1} holographic grating and an Andor Newton DU970P-UVB CCD camera. The 413.1 nm line of a continuous-wave Kr ion laser (Coherent, mod. Innova 300C) was used for excitation. The Rayleigh scattered light was removed using a holographic notch filter (Kaiser Optical Systems). The monochromator slit was set to 120 lm, yielding a resolution of approximately 4 cm^{-1}, with an increment of approximately 0.8 cm^{-1} per data point. RR measurements were done filling a 1-mm-diameter glass capillary with 10 μL of buffered cytc solution (10 μM) and put in a spinning capillary holder under the Raman microscope.

Results and discussion

Diffusionless voltammetry of cytochromes *c* and their CL adducts: oxidation state-dependent conformers and kinetics of species interconversion

The electrochemical behavior of ycc, KtoA and bcc and their adducts with CL immobilized on the DT-coated electrode was studied at different potential scan rates (*v*) (Figs. 1, 2; S2). Cyclic voltammograms (CV) display a maximum of four redox peaks which can be ascribed to the oxidation and reduction of two Fe^{3+}/Fe^{2+} redox couples, attributed to a low-potential (LP) and high-potential (HP) cytc conformers (vide infra), and denoted as I_a, I_c, and II_a, II_c, respectively. The subscripts 'a' and 'c' indicate the anodic and the cathodic peak, respectively. In all cases, cathodic peak currents are linearly dependent on *v*, indicating diffusionless electrochemistry. Cytc was previously shown to bind to hydrophobic SAM-coated electrode surfaces, experiencing conformational changes, which however were not investigated in detail [24]. At low *v*, (Fig. 1) for all species and their CL adducts, peaks I_c and II_a are high intensity while the corresponding anodic and cathodic counterparts

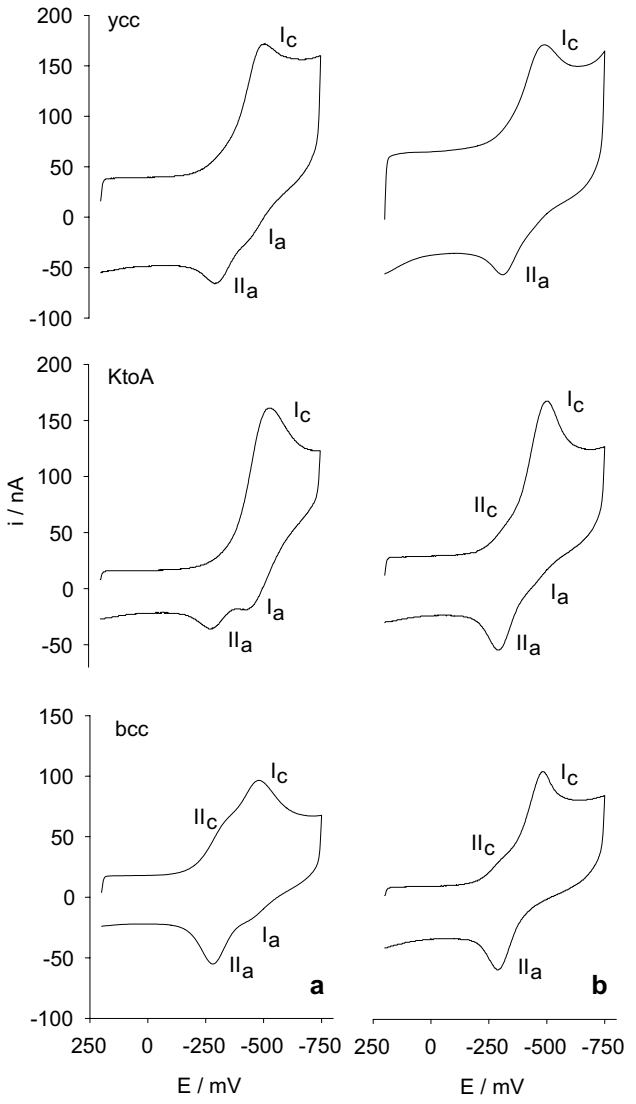

Fig. 1 Cyclic voltammograms at low scan rate for **a** the recombinant *Saccharomyces cerevisiae* yeast iso-1 cytochrome *c* (ycc) and its triple K72A/K73A/K79A variant (KtoA) and cytochrome *c* from beef heart (bcc) immobilized on a hydrophobic SAM of decane-1-thiol (DT) and **b** the corresponding adducts with cardiolipin immobilized under the same conditions. Potentials are vs. SCE. Potential scans started from $E = +0.2$ V. Scan rate, 0.1 V s^{-1}. Working solution: 10 mM Hepes buffer, pH 7. $T = 293$ K

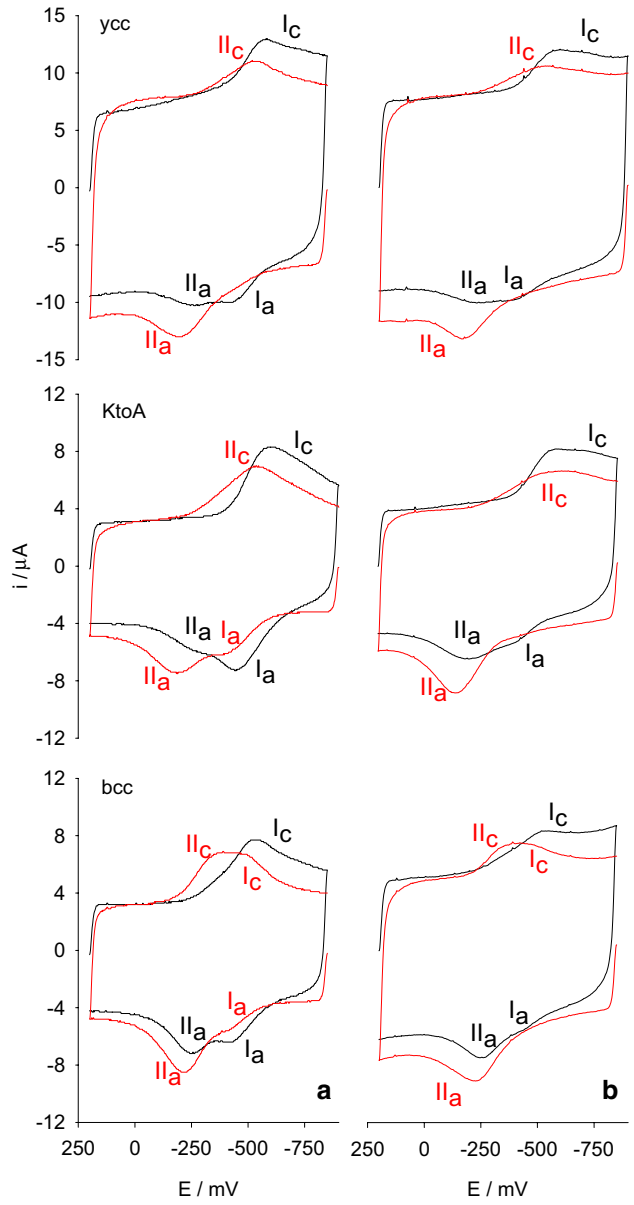

Fig. 2 Cyclic voltammograms at high scan rate for **a** the recombinant *Saccharomyces cerevisiae* yeast iso-1 cytochrome *c* (ycc) and its triple K72A/K73A/K79A variant (KtoA) and cytochrome *c* from beef heart (bcc) immobilized on a hydrophobic SAM of decane-1-thiol (DT); and **b** the corresponding adducts with cardiolipin immobilized under the same conditions. *Black line* cathodic scan started after an oxidizing poise at $E = +0.2$ V followed by an anodic scan. *Red line* anodic scan started after a reducing poise at $E = -0.8$ V followed by a cathodic scan. Potentials are vs. SCE. Scan rate, 20 Vs^{-1}. Working solution: 10 mM Hepes buffer, pH 7. $T = 293$ K

(peaks I_a and II_c, respectively) are much weaker. Only for free bcc (Fig. 1a), both peaks of the two redox couples I and II are clearly visible. Overlapped or poorly resolved peaks were deconvoluted using a homemade program developed on the Origin platform. CVs are independent of whether the potential scan is started from a reducing (negative potentials) or an oxidizing (positive potentials) poise. Moreover, they are reproducible and persist for several cycles, indicating that the protein layer is stable.

These voltammetric responses are affected by the kinetic effects of an oxidation state-dependent conversion between the LP and HP conformers, as shown by the experiments carried out at increasing *v*. In fact, at *v* larger than 0.2 Vs^{-1} starting from a reducing poise (Fig. 2, red line), the anodic scan yields the II_a peak, while its cathodic counterpart, II_c, is observed in the cathodic return. The current of II_c increases with increasing *v* to the detriment of that

of peak I_c, which disappears for v larger than 30 Vs^{-1} (the voltammograms at intermediate scan rates are shown in Figure S2). Conversely, starting from an oxiding poise, the cathodic scan yields peak I_c while at increasing v the new peak I_a, which is the cathodic return of I_c, progressively replaces peak II_a (Fig. 2, black line).

This electrochemical behavior unequivocally indicates that for all free and CL-bound cytochromes two redox state-dependent electrochemically active conformers exist, which are stable in the oxidized and reduced state, corresponding to peak I and II, respectively. These conformers can therefore be termed LP and HP, respectively. The oxidized HP conformer converts with time into the stable oxidized LP conformer while the reduced LP species converts into the reduced HP conformer. It follows, for example, that the cathodic scan started after an oxidizing poise at low v (Fig. 1) yields peak I_c and the following anodic scan contains the peak II_a because of the transition of reduced LP to reduced HP. However, by increasing v we do not give time for this transition and in the anodic scan the current of peak I_a increases with respect to peak II_a (Fig. 2, black line). An analogous reasoning would account for the features of the scans carried out after a reducing poise at low (Fig. 1) and high v (Fig. 2, red line). At v larger than 5 Vs^{-1} the two peaks for both voltammetric signal can be recognized and therefore the individual $E^{\circ\prime}$ values determined (as the average of the cathodic and anodic peak) (Fig. 2; Table 1) (the slow heterogeneous electron transfer rate is most likely responsible for the larger peak separation displayed by the HP couple, namely peaks II_c and II_a, compared to that for the LP couple). The $E^{\circ\prime}$ values for the HP conformer (signal II) are higher than those for the LP conformer by 0.150–0.160 V. The differences are moderately species dependent. Notably, for all species, the $E^{\circ\prime}$ values for both the HP and LP forms of the CL adducts differ (increase) only slightly from those of the uncomplexed species (Table 1). These small effects tell us that no change occurs in axial heme iron coordination upon CL binding. The increase in $E^{\circ\prime}$ values is somewhat larger for the LP form. The observed change in $E^{\circ\prime}$ could be due to either destabilization of the LP (His/His) form in the ferric state by CL binding or stabilization of the corresponding ferrous state by CL. The larger structural flexibility of the ferricytochrome *c* compared to the reduced form shown by the NMR solution structures [25] probably plays a role in the relative stability of the two redox states of the LP form.

The kinetic constant, k, for conformer conversion can be determined using a model proposed by Laviron [26] for an electrochemical reaction followed by a first-order chemical reaction. The rate constants for the oxidized HP to LP transition are listed in Table 1. It turns out that deletion of three lysines in the KtoA variant slows the dynamics of HP to LP switching in the absence of CL compared to the wt protein.

Table 1 Formal reduction potential ($E^{\circ\prime}$) for cytochromes *c* and their CL adducts immobilized on a DT-coated gold electrode, and kinetic constant (k) for the HP to LP transition of the ferric form

Protein	$E^{\circ\prime}$[a]/V	k/s^{-1}[b]
ycc		
LP	−0.253	3.8 ± 0.2
HP	−0.106	
ycc + CL		
LP	−0.226	9.3 ± 0.2
HP	−0.101	
KtoA		
LP	−0.270	0.9 ± 0.1
HP	−0.111	
KtoA + CL		
LP	−0.248	12.8 ± 0.2
HP	−0.106	
bcc		
LP	−0.226	4.7 ± 0.2
HP	−0.081	
bcc + CL		
LP	−0.213	16.0 ± 0.9
HP	−0.077	

Values obtained in 10 Mm Hepes buffer, at pH 7

[a] Vs. SHE, at 293 K; average error on $E^{\circ\prime}$ ± 0.002 V

[b] $T = 293$ K

This result could indicate that the loss of electrostatics on the surface of the KtoA variant strengthens the hydrophobic interaction of KtoA with the SAM surface thereby slowing the interconversion between ligation states. On the other hand, binding to CL increases the HP to LP conversion rate, likely through the weakening of some structural constraints. The fact that the rate increase is the highest for the KtoA variant would suggest that these constraints are at least partially electrostatic in nature and involve the mutated Lys residues near the heme crevice. The similarity between the rates of HP to LP conversion for yeast, bovine and KtoA cytc in the presence of CL could indicate a similar site of interaction with CL almost unaffected by mutation of lysines 72, 73 and 79.

The observed rate constants are lower than that for the Lys to Met switching measured for the reduced alkaline form of mitochondrial cytcs in solution (60 s^{-1} for yeast cytc and 33 s^{-1} for horse cytc) [27], but similar to those for bacterial cytcs (0.98–1.05 s^{-1}) in solution [28]. Conversely, they are quite higher than that for His/His to His/Met conversion for the urea-unfolded K73H mutant immobilized on MUA/MU SAM (0.28 s^{-1}) [8]. Redox state-dependent conformers for ycc-CL in solution at pH 7.4 were also previously found by Bradley et al. [7] through magnetic circular dichroism spectroscopy and potentiometric titrations.

Two ferric conformers were detected in an approximately 60:40 molar ratio whose low-spin heme iron center was assigned a His/Lys and His/OH^- axial ligation, respectively. The reduced adduct was proposed to be predominantly high- spin with a five-coordinate His/− heme iron [7]. We observe that the $E^{\circ\prime}$ value for the present immobilized LP conformer, stable in the oxidized state, for ycc and its KtoA variant is similar. As the variant cannot yield the Lys–Fe–His conformer, it is unlikely that this conformer experiences the His/Lys axial ligation proposed for the solution state.

RR and SERR spectroscopy: effects of protein immobilization on axial heme iron ligation of cytochromes *c* and their CL adducts

Structural insight into the coordination features of the heme center of cytc bound to CL in solution and in the immobilized state can be gained from Resonance Raman (RR) and surface-enhanced resonance Raman (SERR) spectroscopy, respectively [29]. The frequency of a number of bands originating from heme vibrational modes are indeed diagnostic of the iron oxidation and spin state and coordination number [30–33]. In particular, the ν_2, ν_3, ν_4, ν_8, and ν_{10} bands, according to the notation by Abe et al. [34] are taken as marker bands. The Raman shifts and the band intensities in the RR spectrum of oxidized bcc in solution at pH 7, and particularly those at 1,371, 1,501, 1,584, and 1,635 cm^{-1} are typical of the Met–Fe–His axial ligation (Fig. 3a). Wild-type yeast cytc yields a fully comparable spectrum (Figure S3a). For both proteins, the RR spectrum of oxidized cytc–CL shows a slight upshift of the bands in the high-frequency region and an increase of the intensity of the band at 413 cm^{-1} with respect to that at 397 cm^{-1} (Figs. 3b; S3b). Both changes are consistent with the presence of a nonnative Lys–Fe–His heme ligation, as proposed elsewhere [7, 35]. From visual inspection of the spectra, the presence of an additional conformer featuring a hydroxide ion as sixth (axial) ligand proposed previously [7] cannot be neither confirmed nor excluded. Therefore, CL binding to cytc in solution induces a change in the coordination features of the heme center, in agreement with previous work (Scheme 1) [7, 35].

This is not the case for the immobilized state. In fact, the SERRS measurements made on the electrode-immobilized cytochromes and their CL adducts described below show that (a) their heme axial ligation differs from that of the corresponding species in solution and (b) CL binding to cytc does not affect the coordination of the heme center, in full agreement with the electrochemical data discussed above. In fact, SERR spectra obtained for the immobilized cytcs with and without CL display the same conformers (Figs. 3, 4; S3, S4). Therefore, the motional constraints

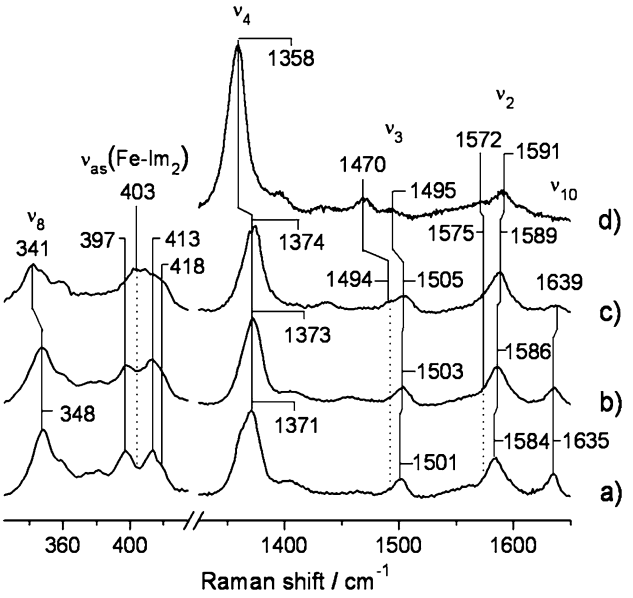

Fig. 3 RR spectra of oxidized beef heart cytc (bcc) (*a*) and its CL adduct (*b*) in aqueous solution pH 7. SERR spectrum of the oxidized (*c*) and the reduced (*d*) bcc-CL adduct adsorbed on a nanostructured Ag electrode coated with a SAM of DT. Spectra (*c*) and (*d*) were obtained at open circuit and −650 mV vs. SCE, respectively. All spectra were normalized with respect to the intensity of the ν_4 band. The intensity of the normalized spectrum (*d*) was multiplied by 2 to better visualize the changes occurring in the ν_3 region. Acquisition parameters were: exposure time = 90 s, 3 accumulations, power on the sample = 1 mW

and the conformational changes induced by protein adsorption on the hydrophobic SAM-coated surface influence the nature of the coordination set of the heme iron for uncomplexed and CL-bound cytochromes. This immobilization-induced change in heme axial coordination was also previously observed for a cytc variant bound on a negatively charged SAM [8].

The SERR spectrum of electrode-immobilized cytc–CL recorded at open circuit (Fig. 3c, 4c; S3c) differs remarkably from that in solution. In particular, a further upshift of the bands in the high-frequency region occurs, along with major changes at low frequencies and the appearance of two bands at 1,494 and 1,575 cm^{-1}. The bands at 1,375, 1,506, 1,589 and 1,639 cm^{-1} and their relative intensities indicate the presence of a six-coordinated low-spin (6cLS) His/His ligated heme center [36]. The prominent band at 403 cm^{-1}, which is typical of the asymmetric stretching of the Fe atom bound to the imidazole N atom of a His residue [ν_{as}(Fe–Im_2)], unequivocally testifies the presence of the His–His ligand set. Moreover, the downshift of the ν_8 band from 348 to 341 cm^{-1} and the concomitant increase of the contribution at 418 cm^{-1} strengthen this assignment [37]. Most notably, the two modes at 1,494 and 1,575 cm^{-1} can be assigned to a five-coordinated high-spin (5cHS)

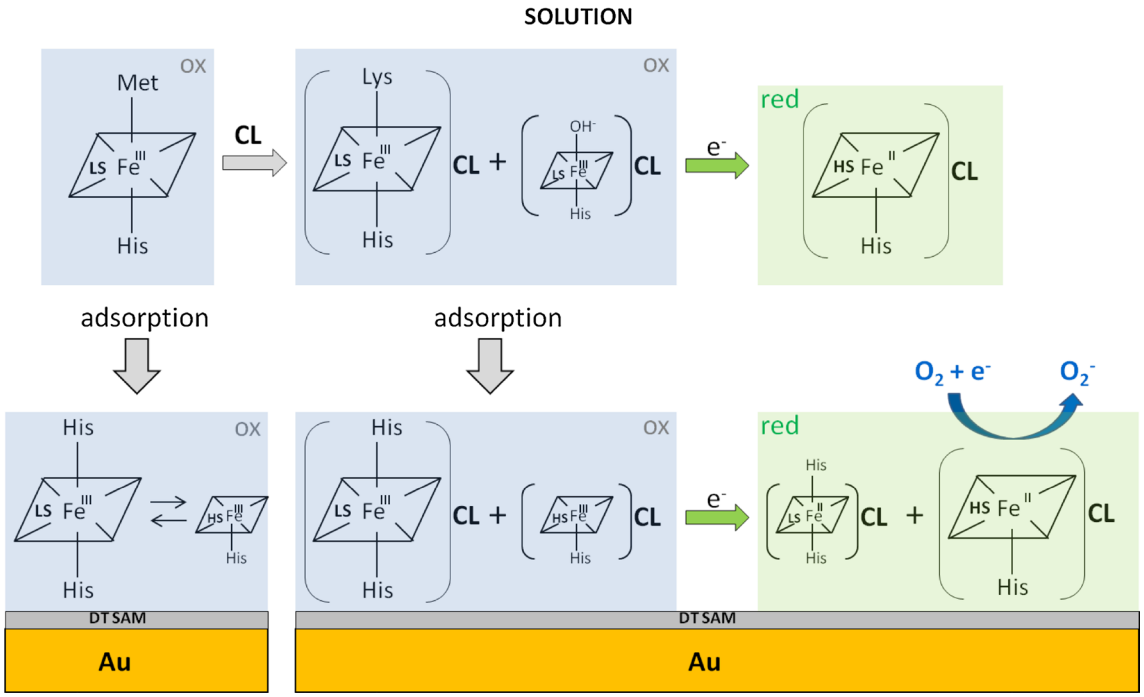

Scheme 1 Cartoon depicting the axial heme ligand coordination for oxidized and reduced cytochrome *c* and its cardiolipin (CL) adduct in solution and adsorbed on the decane-1-thiol SAM-coated gold electrode, at pH 7. The data for the immobilized protein are from this work, while those in solution are from Refs. [7] and [35] and this work as well. The size of the plane representing the heme center symbolizes the abundance of the conformer. Arrows correspond to the processes studied in this work

heme species [36]. Therefore, immobilized ferric cytc–CL appears as a mixture of a prevailing form with a 6cLS His/His ligated heme and another less abundant form featuring a high-spin heme in which the sixth ligand is lacking (Scheme 1). Consistently, a bis-His axial heme ligand set was found previously for human ferricytochrome *c* in a hydrophobic micellar environment [38, 39] His26 and His33 were suggested as candidates to serve as sixth ligand [39]. These residues are distant from the heme iron in the native structure, but their binding could be the result of the large-scale cytc unfolding in the CL adduct [40]. The relative amount of the conformers can be estimated taking into account their cross sections in the ν_3 region. In the case of an equimolar mixture of 5cHS and bis-His conformers, the ν_3 of the oxidized 5cHS is 0.9 times that of the bis-His, while for the reduced species, the ratio is 0.5 [41]. It follows that, while in the oxidized state the amount of 5cHS is slightly less abundant than the bis-His, in the reduced state the 5cHS species is largely dominant, since the band at 1,469 cm^{-1} is stronger than that at 1,494 cm^{-1} (an equimolar mixture is expected to give a band at 1,469 cm^{-1} whose intensity is half that of the band at 1,494 cm^{-1}). This finding is consistent with the coexistence of peaks I_c and II_c in the cathodic scan at low scan rate in the CV for all the cytochromes studied and their CL adducts (Fig. 1). Therefore, it follows that the more thermodynamically stable LP form (peak I) can be assigned a LS six-coordinated His/His center while the HP form (peak II) should correspond to a HS five-coordinated His/− center. The replacement of a Lys by a His residue as a sixth axial heme iron ligand in cytc–CL on passing from the free state in solution to the motionally constrained state on the SAM (mimicking the binding to IMM) would resolve the problem of the peroxidase activity of CL-bound cytc. In fact, it is known that cytc with a His/Lys axial ligation has neither peroxidase activity nor binds dioxygen in the reduced state [42, 43]. Instead, the His/His ligated cytc shows peroxidase activity [44, 45], binds and turns over hydrogen peroxide [46, 47] and catalyzes the reduction of dioxygen to superoxide anion [48]. The latter property is shown indeed by the cytc–CL adducts studied here, as described below. All activities are functional to the peroxidation of CL by cytc in the onset of the apoptotic cascade [5, 6].

The KtoA variant lacks the Lys residues involved in the formation of the Lys–Fe–His heme species. Consistently, the RR spectrum of the CL adduct formed by this variant in solution (Fig. 4b) shows that the heme experiences a His/His axial binding (bands at 1,374, 1,505, 1,588, and 1,639 cm^{-1}) with a minor 5cHS contribution (bands at 1,494 and 1,575 cm^{-1}). This ligand set is maintained in the electrode-immobilized adduct (Fig. 4c), for which the His/His heme ligation becomes even more evident. This

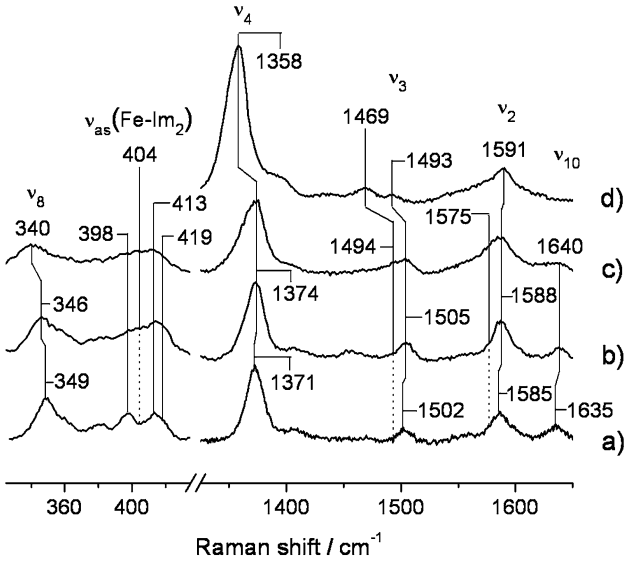

Fig. 4 RR spectrum of the oxidized K72A/K73A/K79A variant of yeast iso-1 cytochrome *c* (KtoA) (*a*) and its CL adduct (KtoA-CL) (*b*) in aqueous solution pH 7. SERR spectrum of the oxidized (*c*) and the reduced (*d*) KtoA-CL adduct adsorbed on a nanostructured Ag electrode coated with a SAM of DT. Spectra (*c*) and (*d*) were obtained at open circuit and −650 mV vs. SCE, respectively. The intensity of the normalized spectrum (*d*) was multiplied by 2 to better visualize the changes occurring in the ν_3 region. Acquisition parameters for spectrum *a* were: exposure time = 120 s, 2 accumulations, power on the sample = 1 mW. Acquisition parameters for spectra *b*, *c* and *d* were: exposure time = 90 s, 3 accumulations, power on the sample = 1 mW

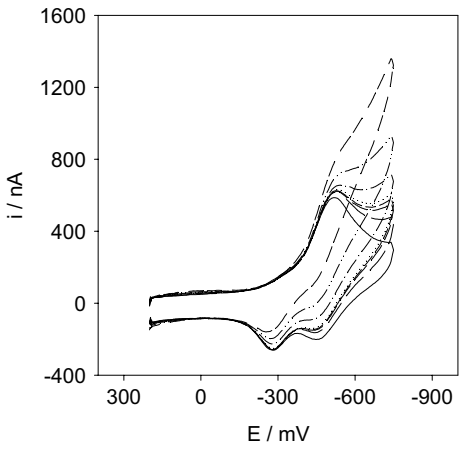

Fig. 5 Cyclic voltammograms for the CL adduct of the K72A/K73A/K79A variant of yeast iso-1 cytocrome *c* immobilized on a DT-coated gold electrode recorded at different exposure times of the electrochemical cell (initially under argon) to air at normal atmospheric pressure. Sweep rate, 0.02 V s^{-1}. $T = 293$ K. The wt yeast and native beef heart species show the same behavior

nicely supports the presence of the His/His ligation set in the immobilized ferric cytc–CL for bovine and yeast cytc. The SERRS spectra for the immobilized cytcs and their CL adducts in the reduced state could only be obtained applying a potential of −0.650 V vs. SCE to the working electrode in a sealed spectroelectrochemical cell flushed with N_2-saturated buffer solution. The spectra, which are identical for all species (Fig. 3d, 4d; S3d, S4d–f), show the persistence of the 6cLS His/His and the 5cHS His/− centers (bands at 1,358, 1,494, 1,591, and 1,469 cm^{-1}, respectively), with a prevalence of the latter form. Therefore, in all cases, cytc reduction at the electrode results in the loss of the sixth ligand from iron coordination and switch to a 5cHS His/− ferrous state (Scheme 1). This form therefore corresponds to the HP conformer, stable in the reduced state, yielding the CV peak II. The $E^{\circ\prime}$ values of these conformers (Table 1) support this assignment. Indeed, the $E^{\circ\prime}$ of the HP conformer is similar to that of immobilized myoglobin, which features a five-coordinated high-spin His/− ligated heme [49]. Both are much higher than the $E^{\circ\prime}$ of the LP conformer (peak I) which resemble those of urea-unfolded cytc [8, 50, 51] and diheme DHC [52] showing a 6c His/His ligated heme. We note that residual O_2 in the cell invariably induced rapid and irreversible desorption of the protein, and the consequent loss of intensity of the SERR signals (not shown). This behavior is relevant because it reproduces cytc release into the intermembrane space following CL peroxidation. Possibly, the dioxygen reduction product, likely the superoxide anion, oxidizes the outer CL chains likely at the double bonds, inducing a conformational change that weakens the hydrophobic interaction with the SAM. An analogous event could occur in vivo where the oxidation process lifts the electrostatic interaction of cytc–CL with IMM. Such a detachment of the reduced adduct from the DT-coated electrode is confirmed by the CV data described below showing cytc–CL-induced catalytic dioxygen reduction.

Catalytic dioxygen reduction by electrode-immobilized cytc–CL adduct

Figure 5 shows the electrochemical response of cytc–CL immobilized on the DT-coated gold electrode in the presence of increasing dioxygen concentration (obtained by increasing the time of exposure of the electrochemical cell, initially under argon, to air). The corresponding increase in intensity of the cathodic peak with a concomitant decrease in the anodic current indicates that immobilized cytc–CL under these conditions is able to reduce dioxygen electrocatalytically at the heme iron, as hypothesized for reduced cytc–CL in solution [7] and observed previously for unfolded cytochrome *c* or variants containing a five-coordinated heme–iron center (Scheme 1) [48, 53, 54]. This ability is most likely related to the high affinity of dioxygen for the ferrous heme and the concomitant reduction-induced weakening of the axial bond of the sixth (axial) His ligand

to the heme iron which favors ligand substitution [48]. The mechanism for O_2 reduction likely implies an oxidative addition of O_2 to Fe-(II), yielding a Fe(III)–O_2^- derivative, which then dissociates [48]. The biocatalytic effect is progressively lost upon repeated cycling in the presence of dioxygen, resulting in current fading. This effect was also observed previously for immobilized M80A ycc variant [53, 54], and put in relation with oxidation of the SAMs caused by the superoxide anion (which would result in protein desorption). However, other factors could be involved, among which the above mentioned oxidation of the CL acyl chains.

Conclusions

Binding of cytc to CL, which is a component of the inner mitochondrial membrane, has been mimicked by immobilizing the adduct on a hydrophobic SAM-coated electrode surface. Diffusionless voltammetry and SERR spectroscopy showed that immobilized cytc and its CL adduct feature an equilibrium between a 6cLS His/His and a 5cHS His/− coordination states. The former prevails in the oxidized and the latter in the reduced state. It is found that CL binding makes the conversion between the oxidation state-dependent conformers faster. Axial heme coordination in the adduct changes compared to the solution state, particularly for the ferric state. These findings suggest that restrictions of motional freedom due to interaction with the membrane could be one additional factor playing in the mechanism of cytc unfolding and its reactivity. However, we cannot rule out the possibility that the charged surface of a CL-containing membrane might introduce different perturbations to the distribution of heme ligation states than observed here for a hydrophobic SAM surface.

Moreover, the fact that, contrary to the solution state, the immobilized ferrous adduct is able to catalytically reduce dioxygen suggests reconsideration of the role of cytc-mediated peroxidation in the apoptosis cascade. High levels of superoxide ion can trigger cell death and mitochondria undergo spontaneous bursts of superoxide generation, termed “superoxide flashes” [55–57]. Individual flashes are triggered by transient openings of the mitochondrial permeability transition pores stimulating superoxide production by the electron transport chain and constitute early mitochondrial signals that initiate oxidative stress-related apoptosis in a context-dependent manner [57]. The exact mechanisms underlying superoxide flash generation, regulation and function remain uncertain. However, a burst of superoxide flash activity during reoxygenation of cardiomyocytes after hypoxia has been recently reported [55, 57], suggesting a direct involvement of O_2 in superoxide ion generation during pre-apoptotic processes in mitochondria.

Acknowledgments This work has been supported by the Italian Ministry of University and Research (PRIN 2009 prot. N. 20098Z4M5E_002) [M.B.], DM acknowledges the Netherlands Organisation for Scientific Research (NWO) Grant 722.011.003. AR acknowledges the LaserLaB Access Program (project number LLAMS001927, LASERLAB-EUROPE Grant agreement No. 284464, EC’s Seventh Framework Programme).

References

1. Battistuzzi G, Borsari M, Cowan JA, Ranieri A, Sola M (2002) J Am Chem Soc 124:5315–5324
2. Bowler EB (2012) Characterization of the denatured state. In: Egelman EH (eds) Comprehensive biophysics, vol 3. Elsevier B.V., Amsterdam, pp 72–114
3. Battistuzzi G, Borsari M, Rossi G, Sola M (1998) Inorg. Chim. Acta 272:168–175
4. Monari S, Battistuzzi G, Borsari M, Di Rocco G, Ranieri A, Sola M (2009) J Phys Chem B 113:13645–13653
5. Kagan VE, Tyurin VA, Jiang J, Tyurina YY, Ritov VB, Amoscato AA, Osipov AN, Belikova NA, Kapralov AA, Kini V, Vlasova II, Zhao Q, Zou M, Di P, Svistunenko DA, Kurnikov IV, Borisenko GG (2005) Nat Chem Biol 1:223–232
6. Belikova NA, Vladimirov YA, Osipov AN, Kapralov AA, Tyuri VA, Potapovich MV, Basova LV, Peterson J, Kurnikov IV, Kagan VE (2006) Biochemistry 45:4998–5009
7. Bradley JM, Silkstone G, Wilson MT, Cheesman MR, Butt JN (2011) J Am Chem Soc 133:19676–19679
8. Ranieri A, Bortolotti CA, Battistuzzi G, Borsari M, Paltrinieri L, Di Rocco G, Sola M (2014) Metallomics 6:874–884
9. Rytömaa M, Kinnunen PKJ (1995) J Biol Chem 270:3197–3202
10. Kalanxhi E, Wallace CJA (2007) Biochem J 407:179–187
11. Sinibaldi F, Howes BD, Piro MC, Polticelli F, Bombelli C, Ferri T, Coletta M, Smulevich G, Santucci R (2010) J Biol Inorg Chem 15:689–700
12. Basova LV, Kurnikov IV, Wang L, Ritov VB, Belikova NA, Vlasova II, Pacheco AA, Winnica DE, Peterson J, Bayir H, Waldeck DH (2007) Kagan VE. Biochemistry 46:3423–3434
13. Perhirin A, Kraffe E, Marty Y, Quentel F, Elies P, Gloaguen F (2013) Biochim Biophys Acta General Subjects 1830:2798–2803
14. Sinibaldi F, Droghetti E, Polticelli F, Piro MC, Di Pierro D, Ferri T, Smulevich G, Santucci R (2011) J Inorg Biochem 5:1365–1372
15. Battistuzzi G, Borsari M, De Rienzo F, Di Rocco G, Ranieri A, Sola M (2007) Biochemistry 46:1694–1702
16. Rosell FI, Ferrer JC, Mauk AG (1998) J Am Chem Soc 120:11234–11245
17. Pollock WBR, Rosell FI, Twitchett MB, Dumont ME, Mauk AG (1998) Biochemistry 37:6124–6131
18. Cutler RJ, Pielak GJ, Mauk AG, Smith M (1987) Protein Eng 1:95–99
19. Kapetanaki SM, Silkstone G, Husu I, Liebl U, Wilson MT, Vos MH (2009) Biochemistry 48:1613–1619
20. Gopal D, Wilson GS, Earl RA, Cusanovich MA (1998) J Biol Chem 263:11652–11656
21. Osheroff N, Brautigan DL, Margoliash E (1980) Proc Natl Acad Sci USA 77:4439–4443
22. Bonifacio A, Millo D, Keizers PHJ, Boegschoten R, Commandeur JNM, Gooijer C, van der Zwan G (2008) J Biol Inorg Chem 13:85–96
23. Millo D, Bonifacio A, Ranieri A, Borsari M, Gooijer C, van der Zwan G (2007) Langmuir 23:4340–4345
24. Chen X, Ferrigno R, Yang J, Whitesides GM (2002) Langmuir 18:7009–7015

25. Banci L, Bertini I, Rosato A, Varani G (1999) J Biol Inorg Chem 4:824–837
26. Laviron E (1972) J Electroanal Chem 35:333–342
27. Barker PD, Mauk AG (1992) J Am Chem Soc 114:3619–3624
28. Battistuzzi G, Borsari M, Ferretti S, Sola M, Soliani E (1995) Eur J Biochem 232:206–213
29. McNay G, Eustace D, Smith WE, Faulds K, Graham D (2011) Appl Spectrosc 65:825–837
30. Spiro TG, Czernuszewicz RS, Li X (1990) Coord Chem Rev 100:541–571
31. Kitagawa T, Ozaki Y (1987) Struct Bonding 64:71–114
32. Spiro TG, Li X (eds) (1990) Biological applications of Raman spectroscopy. Wiley, New York
33. Procyk AD, Bocian DF (1992) Annu Rev Phys Chem 43:465–496
34. Abe M, Kitagawa T, Kyogoku Y (1978) J Chem Phys 69:4526–4534
35. Sinibaldi F, Howes BD, Droghetti E, Polticelli F, Piro MC, Di Pierro D, Fiorucci L, Coletta M, Smulevich G, Santucci R (2013) Biochemistry 52:4578–4588
36. Oellerich S, Wackerbarth H, Hildebrandt P (2002) J Phys Chem B 106:6566–6580
37. Santoni E, Scatragli S, Sinibaldi F, Fiorucci L, Santucci R, Smulevich G (2004) J Inorg Biochem 98:1067–1077
38. Simon M, Metzinger-Le Meuth V, Chevance S, Delalande O (2013) Bondon. J Biol Inorg Chem 18:27–38
39. Oellerich S, Wackerbarth H, Hildebrandt P (2003) Eur Biophys J 32:599–613
40. Hong Y, Muenzner J, Grimm SK, Pletneva EV (2012) J Am Chem Soc 134:18713–18723
41. Hildebrandt P, Stockburger M (1989) Biochemistry 28:6710–6721
42. Diederix REM, Ubbink M, Canters GW (2002) Biochemistry 41:13067–13077
43. Ranieri A, Bernini F, Bortolotti CA, Bonifacio A, Sergo V, Castellini E (2011) Langmuir 27:10683–10690
44. Lightning LK, Huang H-W, Moënne-Loccoz P, Loehr TM, Schuller DJ, Poulos TL, de Ortiz Montellano PR (2001) J Biol Chem 276:10612–10619
45. Prasad S, Maiti NC, Mazumdar S, Mitra S (2002) Biochim Biophys Acta Prot Struct Mol Enzymol 1596:63–75
46. Bortolotti CA, Paltrinieri L, Monari S, Ranieri A, Borsari M, Battistuzzi G, Sola M (2012) Chem Sci 3:807–810
47. Ranieri A, Battistuzzi G, Borsari M, Bortolotti CA, Di Rocco G, Monari S, Sola M (2012) Electrochem Commun 14:29–31
48. Tavagnacco C, Monari S, Ranieri A, Bortolotti CA, Peressini S, Borsari M (2011) Chem Commun 47:11122–11124
49. Liu X, Huang Y, Zhang W, Fan G, Fan C, Li G (2005) Langmuir 21:375–378
50. Monari S, Millo D, Ranieri A, Di Rocco G, van der Zwan G, Gooijer C, Peressini S, Tavagnacco C, Hildebrandt P, Borsari M (2010) J Biol Inorg Chem 15:1233–1242
51. Monari S, Ranieri A, Bortolotti CA, Peressini S, Tavagnacco C, Borsari M (2011) Electrochim Acta 56:6925–6931
52. Di Rocco G, Ranieri A, Bortolotti CA, Battistuzzi G, Bonifacio A, Sergo V, Borsari M, Sola M (2013) Phys Chem Chem Phys 15:13499–13505
53. Casalini S, Battistuzzi G, Borsari M, Ranieri A, Sola M (2008) J Am Chem Soc 130:15099–15104
54. Casalini S, Battistuzzi G, Borsari M, Bortolotti CA, Ranieri A, Sola M (2008) J Phys Chem B 112:1555–1563
55. Wang W, Fang H, Groom L, Cheng A, Zhang W, Liu J, Wang X, Li K, Han P, Zheng M, Yin J, Wang W, Mattson MP, Kao JP, Lakatta EG, Sheu SS, Ouyang K, Chen J, Dirksen RT, Cheng H (2008) Cell 134:279–290
56. Ma Q, Fang H, Shang W, Liu L, Xu Z, Ye T, Wang X, Zheng M, Chen Q, Cheng H (2011) J Biol Chem 286:27573–27581
57. Wang X, Jian C, Zhang X, Huang Z, Xu J, Hou T, Shang W, Ding Y, Zhang W, Ouyang M, Wang Y, Yang Z, Zheng M, Cheng H (2012) J Mol Cell Cardiol 52:940–948